J Nanostruct 13(2): 597-607, Spring 2023

RESEARCH PAPER

Synthesis and Characterization of Hybrid-Nano Graphene Oxide Composites Membranes for Water Treatment

*Sammah Naeem Ghazi, Safaa Sabri Najim *; Ahmed Majeed Abbas*

Department of Chemistry, College of Science, University of Misan, Maysan, Iraq

ARTICLE INFO

Article History:
Received 19 January 2023
Accepted 27 March 2023
Published 01 April 2023

Keywords:
Membrane
Nano-graphene oxide-Cysteine
Nano-graphene oxide-chitosan
Nano-graphene oxide-methionine
Trace metals

ABSTRACT

Synthesis and characterization of nano-graphene oxide (NGO), nano-graphene oxide-chitosan (NGO-CS), nano-graphene oxide-Methionine (NGO-M) and nano-graphene oxide-Cysteine (NGO-C) composites, by FT-IR to determine the formation of the new bonds, XRD to find out the particles size (7.4, 10.8, 16.83 and 19.52 nm) for NGO, NGO-CS, NGO-M and NGO-C composites respectively, through Debye-Scherrer equation. The fabrication of NGO, CS, NGO-CS, NGO-M and NGO-C membranes by vacuum filtration and determining of the average pore sizes by FESEM (52.31-613.20), (63.14-972.40), (49.53-347.50), (84.8-326.00) and (55.32-147.01) nm respectively. In the membranes used to separate an organic pollutant (BPB dye), the removal percentages are (85.65%, 95.35%, 98.52%, 86.91% and 92.61%) respectively, and the best membrane was NGO-CS. These membranes also used to separate trace heavy metals as inorganic pollutants, Ni^{+2}, Cd^{+2}, Co^{+2}, Cu^{+2} and Pb^{+2} ions from aqueous solutions, the best membrane was (NGO-CS, CS, NGO-CS, NGO-M and NGO-CS) for each metal ions respectively, while the removal percentages were as follows (46.43%, 52.2%, 68%, 17%, 66%, 47% and 67.04 %) respectively.

How to cite this article
Ghazi S N., Najim S. S., Abbas A. M. Synthesis and Characterization of Hybrid-Nano Graphene Oxide Composites Membranes for Water Treatment. J Nanostruct, 2023; 13(2):597-607. DOI: 10.22052/JNS.2023.02.030

INTRODUCTION

There are essentially two types of chemical contamination: inorganic and organic contaminants [1]. Industrial processes release significant amounts of toxic heavy metals into the environment. Heavy metals like copper, chromium, cadmium, nickel, lead, zinc, and mercury are released into industrial wastewater and urban sewage, as a result of several processes, including mining, battery production, and plating [2]. Heavy metals cannot be broken down or destroyed [3]. Buildup in the human body may impair the bones, central nervous system, renal structure and function, and hematological issues since they tend to collect in living organisms and can cause several deadly diseases. Moreover, since heavy metals are toxic, even at deficient concentrations, they can adversely affect the metabolic reactions in living organisms [4]. The dyes and printing of textiles consume around 8000 chemical compounds, the majority of which have detrimental impacts on health either directly or indirectly [5]. The introduction of dyes into the water system causes several health and environmental problems [6,7]. Bromophenol blue dye (3', 3', 5', 5''-tetrabromophenolsulfonaphthalein), known for its potentially genotoxic derivatives [8], was used as a model molecule and contaminant in

* *Corresponding Author Email: safchem2000@uomisan.edu.iq*

this study. Triphenylmethane dyes are xenobiotic aromatic substances, allegedly very harmful to mammalian cells and to be carcinogenic and mutagenic to humans. The membrane filtration technique has drawn more attention than other treatment technologies for water purification. The effectiveness of the membrane technique, which is commonly recognized as an effective and affordable approach for treating wastewater, is significantly influenced by the selectivity and permeability of the membrane materials. Due to excessive energy consumption brought on by membrane fouling and other problems, this method was not widely used. The technique has a large initial outlay need and a clogging risk. The frequent replacement of the membrane is yet another disadvantage of this method. This method is suitable when the effluent has a low dye content. Membrane filtration can be used with other methods for treating wastewater. The common membrane filtration types are Micro- Filtration (MF), Ultra-Filtration (UF), Nano-Filtration (NF), and Reverse Osmosis (RO), they are used for color removal, BOD reduction, salt reduction and polyvinyl acetate (PVA) recovery, as well as organic pollutants and microorganisms found in wastewater. The desired quality of the final effluent influences the membrane process choice [9]. Numerous studies have suggested that adding carbonaceous nanoparticles to membranes can increase their selectivity, permeability, and resistance to fouling. Only particles with a diameter of 1–10 m may be filtered using microporous membranes, which restricts their usage in water purification. The majority of contaminants (1–10 nm), including metallic ions, organic compounds, salts, and microorganisms, may be removed from wastewater by using nano porosity membranes, which have demonstrated good performance for water purification [10]. Numerous inorganic, organic, and inorganic-organic hybrid materials have been used to build high-performance nano-porous membranes for water filtration. For instance, water desalination utilizing single-layer nano-porous graphene [11]. There are three broad categories of nano-porous membranes for water filtration based on their material composition: inorganic membranes, organic membranes, and inorganic-organic hybrid membranes [12]. Inorganic membranes, organic membranes, and inorganic-organic hybrid membranes. Inorganic membranes are mostly composed of ceramics (Al_2O_3, TiO_2, ZrO_2, SiO_2, TiO_2-SiO_2, Al_2O_3-SiC), graphene, and other materials [13], and carbon nanotubes (CNTs). Organic membranes are primarily composed of polymeric substances like polyvinyl alcohol (PVA), polyimide (PI), polypropylene (PP), polyethersulfone (PES), cellulose acetate (CA), cellulose nitrates, polysulfone (PSU), polyvinylidene fluoride (PVDF), polyacrylonitrile (PAN), polytetrafluoroethylene (PTFE), and biomacromolecules. Typically, inorganic elements like metals, metal oxides, or carbon-based compounds are commonly incorporated into polymeric matrices to form inorganic-organic hybrid membranes that has led to advancements in nanotechnology and materials science, facilitating the design of novel nanocomposites with enhanced functionalities [14].

The objectives of this study are to synthesize and characterize nano-graphene oxide (NGO), nano-graphene oxide-chitosan (NGO-CS), novel nano-graphene oxide-Methionine (NGO-M), and nano-graphene oxide-Cysteine (NGO-C) composite membranes for the separation of BPB dye and some heavy metal ions.

MATERIALS AND METHODS

Instrumentation

UV-Vis. Spectrophotometer, FT-IR (Shimadzu FT-IR-8400S), XRD (Philips PW1730), FESEM (Fei inspect f 50), FAA (Aurora Al -1200), Ultrasonic Probe Sonicator (Sino Sonics FSFJY92-IIN), Ultrasonic Bath Sonicator (Daihan Scientific WHC-A10H) and HORIBA SZ-100.

Synthesis of Nano Graphene Oxide

Modified Hummer's technique used for the synthesis of Nano Graphene Oxide (NGO) [15], our previous work [16]. Added 23 mL of cooled (0° C) concentrated sulphuric acid into a beaker, along with 0.60 g of graphite, and 0.50 g of sodium nitrate, stirred for 15 minutes. Progressively added 3.0 g of potassium permanganate to the suspension, turning it black, and continued stirring for 30 minutes on an ice bath to maintain the reaction temperature below 20°C. The reaction beaker was swirling to eliminate the sulphate ions, in a water bath for two hours at 35°C, to keep continuous contact between the reactants. The suspension turned a deep brown color. Then, 100 mL of heated deionized water was added, followed by 10 mL of 30% hydrogen -peroxide, added progressively using a dropper. After 15

minutes, an additional 50 mL of deionized water was gradually added using a dropper over a hot plate magnetic stirrer. The suspension was rinsed with warm hydrochloric acid (5% v/v) to eliminate sulphate ions as tested by $BaCl_2$, the suspension was centrifuged at 4000 rpm for 5 minutes, and the precipitate was washed with deionized water until the pH became 7.0. The product (graphene oxide) was dried in an oven for one hour at 60˚ C. A probe sonicator was used to sonicate 50 mL of N, N-di methyl formamide with 0.5 g of graphene oxide for 30 minutes to produce high-quality nanographene oxide sheets, and deagglomeration, decreasing the particle size and surface functionalization. The suspension was separated by centrifugation at 4000 rpm for 10 minutes, the residue was dried in an oven at 60° C for one hour.

Synthesis of (NGO-CS) Hydrogel Composite

Dissolved 1.0 g of chitosan biopolymer in 50.0 mL of (1%) v/v acetic acid, [17-19] stirred until it became a homogeneous solution. Nano graphene oxide 5.0 mg was added to a small portion of deionized water, sonicated by bath sonicator for 2 min. for dispersion, the NGO suspension was gradually added to the chitosan solution, stirring the mixture for 10 minutes to increase the rate of the reaction, keep dispersion and avoid agglomeration. The mixture was sonicated for 30 min. to remove bubbles. The NGO-CS solution was injected by syringe needle (60 drops/min.), 10 cm above sodium hydroxide solution 500 ml (0.5 mol/L), the resulting NGO-CS microspheres kept stirred slowly in the solution for 4 hrs., filtered using a Buechner funnel with perforated aluminum foil sheet, washed with (D.W) until the pH became neutral, dried for 48 hrs. at room temperature, brown beads formed [20].

Synthesis of NGO-M Composite

In a beaker 0.5 g of NGO was added to 50.0 ml DMF as a stable dispersion, ultra-sonicated 30 min., and 1.5 g of methionine amino acid was added to increase the opportunity of amino groups of methionine to react with the carboxyl groups of nanographene oxide, ultra-sonicated for 30 min. The suspension was heated for 30 min. into a microwave (140 W), washed with anhydrous ethanol 200.0 mL several times, then by D.W and ethanol. The final result was the formation of black powder which was dried at 70°C for 6 hrs, our previous work [21] only, [22].

Synthesis of NGO-C Composite

In a beaker 0.5 g of NGO was added with 50 ml DMF, ultra-sonicated for 30 min., 1.21 g of cysteine amino acid was added, ultra-sonicated (30 min.), the suspension heated for 30 min. in a microwave (140 W), washed by anhydrous ethanol 200.0 mL several times, then by D.W and ethanol, the final result was the formation of black powder and dried at 70°C for 6 hrs. our previous work [21], [22].

Membranes fabrication

NGO membrane

NGO membrane (100 ppm) was fabricated by adding 5 mg of NGO powder to 50 ml deionized water, sonicated by bath sonicator (30 ℃ for 2 min.) for dispersion, filtered by using a vacuum pump (-15 psi) with cellulose nitrate membrane filter as a substrate (pores 0.22 µm). as shown in

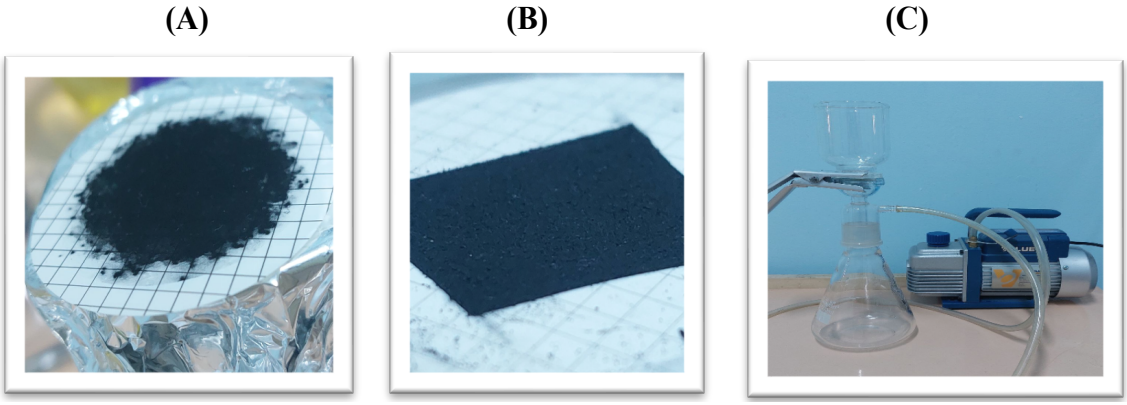

Fig. 1. (A), (B) NGO membrane on substrate (cellulose nitrate), (C) Vacuum flirtation pump apparatus

Fig. 1.

CS membrane

CS membrane (100 ppm) fabricated by dissolving 5.0 mg of chitosan polymer in 50.0 ml of 1% acetic acid[19], filtered by vacuum filtration (-15 psi) over a cellulose nitrate membrane filter as a substrate (pores 0.22 µm).

NGO-CS membrane

NGO-CS membrane (100 ppm) fabricated by dissolving 2.5 mg of the chitosan polymer in 50.0 ml of 1% acetic acid [19], 2.5 mg of nanographene oxide was added, sonicated by ultrasonic bath (30 ℃ for 2 min.), filtered using vacuum filtration with a cellulose nitrate membrane filter as a substrate (pores 0.22 µm).

NGO-M membrane

NGO-M membrane (100 ppm) was fabricated by adding 5.0 mg of the composite to 50.0 ml of deionized water (D.W) and subjected to ultrasonic bath treatment at 30 ℃ for 2 minutes to achieve dispersion. for dispersion, filtered by vacuum filtration (-15 psi) with a cellulose nitrate membrane filter as a substrate (pores 0.22 µm).

NGO-C membrane

NGO-C membrane (100 ppm) was fabricated by adding 5.0 mg of composite to 50.0 ml of D.W, sonicated by an ultrasonic bath (30 ℃ for 2 min. for dispersion, filtered by vacuum filtration (-15 psi) with a cellulose nitrate membrane filter as a substrate (pores 0.22 µm).

Preparation of stock solutions

Stock Solution of Bromophenol blue dye (1000 ppm)

A stock solution of 3',3",5', and 5" tetrabromophenolsulfonphthalein (BPB) (M_{wt} = 669.98 g/mol) was prepared by dissolving 100 mg in deionized water into a beaker, transferred quantitatively

to the volumetric flask (100 mL), filled up to the mark with D.W. By serial dilution of the stock solution, the working standard solutions were prepared.

Stock Solution of Cobalt (1000 ppm)

Cobalt sulphate $CoSO_4.7H_2O$ (0.4769 gm) dissolved in a small amount of (5% HCl) into a beaker (50 ml), transferred quantitatively to a volumetric flask (100 mL) filled up to the mark with deionized water. By serial dilution of the stock solution, the working standard solutions were prepared.

Stock Solution of Nickel (1000 ppm)

Nickel sulphate $NiSO_4.6H_2O$ (0.4476 gm) dissolved in a small volume of (5% HCl) into a beaker (50 ml) and transferred quantitatively to a volumetric flask (100 mL) filled up to the mark with deionized water. By serial dilution of the stock solution, the working standard solutions were prepared.

Stock Solution of Copper (1000 ppm)

Copper sulphate $CuSO_4.5H_2O$ (0.3927 gm) dissolved in a small volume of (5% HCl) into a beaker (50 ml), transferred quantitatively to a volumetric flask (100 mL) filled up to the mark with deionized water. By serial dilution of the stock solution, the working standard solutions were prepared.

Stock Solution of Cadmium (1000 ppm)

Cadmium sulphate $CdSO_4.8H_2O$ (0.2281 gm) dissolved in a small volume of (5% HCl) into a beaker (50 ml), transferred quantitatively to a volumetric flask (100 mL) filled up to the top mark with deionized water. By serial dilution of the stock solution, the working standard solutions were prepared.

Stock Solution of Lead (1000 ppm)

Lead nitrate $Pb(NO_3)_2$ (0.1598 gm) dissolved in a small volume of (5% HCl) into a beaker (50 ml) and transferred quantitatively to a volumetric flask (100 mL) filled up to the mark with deionized water. By serial dilution of the stock solution, the working standard solutions were prepared.

RESULT AND DISCUSSION

Fourier transform infrared spectroscopy (FT-IR)

The FT-IR spectrum of nanographene oxide (NGO) as shown in Fig. 2 (A) broad band observed at 3000-3700 cm^{-1} represents the stretching vibration of OH in carboxylic and alcohol groups [16], while the band at 3124.68 cm^{-1} refers to aromatic C-H stretch of NGO.

Peaks appeared at 1712.79 cm-1 and 1678.07 cm^{-1} which can be assigned to vibration stretching C=O of carboxylic groups and C=C on the basal plan of NGO sheets respectively. The peaks that

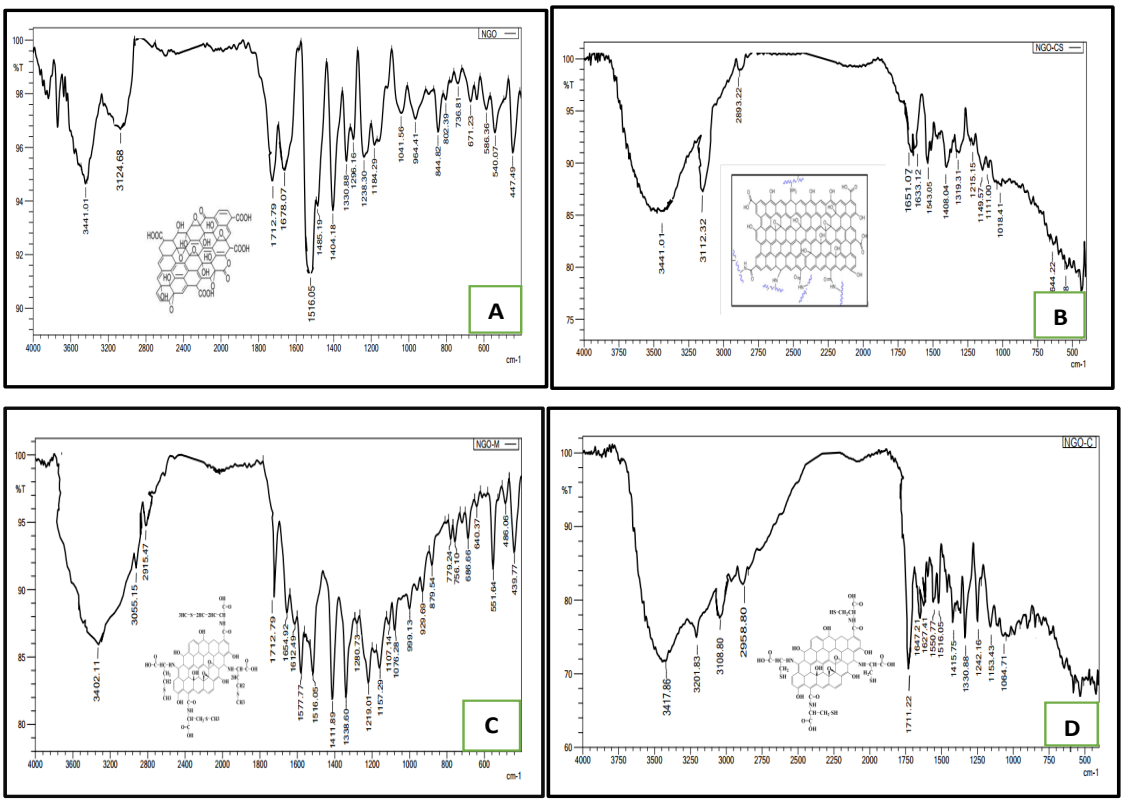

Fig. 2. FT-IR spectrum of (A)NGO, (B) NGO-CS, (C) NGO-M, (D) NGO-C composite

appeared at 1516.05 cm^{-1} refer to epoxy group C-O-C. The FT-IR spectrum of nanographene oxide-chitosan composite (NGO-CS) as shown in Fig. 2 (B) appeared peak refers to the carbonyl of amides group(-NHC=O) at 1651.07 cm^{-1} (This observation can be related to the reaction of carboxyl groups of NGO with amino groups of CS). The band at 1543.05 cm^{-1} could be attributed to C-N of NH II groups as a result of the interaction between the epoxy groups in the NGO and the amino groups in the CS [23]. The observed peak at 2893.22 cm^{-1} is attributed to the C-H aliphatic of CS while, the discernible peak at 3112.32 cm^{-1} can be ascribed to aromatic C-H stretch of NGO the broad peak of OH groups at 3000-3700 cm^{-1} might be due to formation of hydrogen bonding during interaction of NGO and CS. The FT-IR spectrum of nanographene oxide-methionine composite (NGO-M) as shown in Fig. 2 (C) the broad band observed at 3000-3700 cm^{-1} can be attributed to the stretching vibration of O-H groups which is overlapped with N-H, while the band at 3055.15 cm^{-1} and 2915.47 cm^{-1} corresponds to the asymmetric stretching vibrations of aromatic C-H of NGO and aliphatic C-H for the amino acid (methionine), respectively. While the sharp peak at 1712.79 cm^{-1} corresponds to C=O of carboxylic groups. Two peaks appeared at 1654.92 cm^{-1} and 1612.49 cm^{-1} the first peak represents C=O stretching vibrations of -NHCO results from the interaction of the COOH group of NGO with the $-NH_2$ of methionine, while the second peak represents C=C mode of the sp^2 carbon skeletal network of NGO. The eared band at 1516.05 cm^{-1}, could be attributed to C-N of NH II groups formed due to the reaction between amino groups of methionine and epoxy groups of NGO. The FT-IR spectrum of nanographene oxide-cysteine composite (NGO-C) as shown in Fig. 2 (D), The band observed at 3000-3700 cm^{-1} can be attributed to the stretching vibration of O-H groups which is overlapped with N-H stretching vibration, while the band at 3108.80 cm^{-1} and 2958.80 cm^{-1} corresponded to the asymmetric stretching vibrations of aromatic C-H of NGO and aliphatic C-H for amino acid (cysteine), respectively. While the sharp peak at 1711.22 cm^{-1} corresponds to C=O of carboxylic groups [24]. absorption appeared band at 1647.21

cm^{-1} represents the C=C stretching mode of the sp^2 carbon skeletal network of NGO, while the peak at 1550.77 represents to C-N of NH II groups as a secondary amine formed due to reaction between amino groups of cysteine and epoxy group of NGO. The S-H group of cysteine gives a sharp peak at 3201.83 cm^{-1}.

X-ray diffraction spectroscopy

The XRD spectrum was measured in a range of (5°-80°) of 2θ at 0.154 nm (copper source). The XRD peaks of NGO appeared at (2θ=11.1297°) high intensity corresponding to interlayer spacing of (d=7.94350A°), (2θ= 42.4972°) low intensity with interlayer spacing of (d=2.12546 A°) and (2θ= 9.1074°) low intensity with interlayer spacing of (d=9.70232 A°), as shown in Fig. 3(A), The obtained results agree with the previous studies[25] [26]. As for NGO-CS composite appeared at (2θ=20.3255°) high intensity corresponding to interlayer spacing of (d=4.36929 A°) and (2θ= 35.4690°) low intensity with interlayer spacing of (d=2.53092 A°) as shown in Fig. 3 (B), the main peaks of NGO are disappeared by react with chitosan (CS) proved the presence pure phase of the synthesized NGO-CS composite so the results agree with the previous studies[27]. The NGO-M composite appeared at (2θ= 34.02°) high intensity corresponding to the interlayer spacing of (d=2.63 A°), (2θ = 38.80°) medium intensity with an interlayer spacing of (d=2.36 A°), (2θ= 48.86°) medium intensity with an interlayer spacing of (d=1.86 A°), (2θ= 54.73°) low intensity with an interlayer spacing of (d=1.67 A°) and (2θ= 55.35°) low intensity with an interlayer spacing of (d=1.56 A°) as shown in Fig. 3 (C), while NGO-C composite is appeared at (2θ= 34.05°) medium intensity corresponding to interlayer spacing of (d=2.63 A°), (2θ= 38.80°) low intensity with interlayer spacing of (d=2.36 A°), (2θ= 48.86°) low intensity with an interlayer spacing of (d=1.86 A°), (2θ= 54.73°) low intensity with an interlayer spacing of (d=1.67 Å, (2θ= 55.35°) low intensity with an interlayer spacing of (d=1.56 A°), (2θ= 62.15°) low intensity with an interlayer spacing of (d=1.49 A°) and (2θ= 65.24°) low intensity with an interlayer spacing of (d=1.43 A°) as shown in Fig. 3 (D). The peaks appear at several angles compared to the NGO, this shows that the modification process was successful in attaching methionine and cysteine to the NGO surface. The particle size is calculated by Debye-Scherrer question 1 [2].

$$D = \frac{K\lambda}{\beta \cos \theta}$$

Where, D: particle size, K: Scherrer's constant equal 0.9, λ: wavelength of the X-ray radiation source, β: full width at half maximum (FWHM), θ:X-ray diffraction angle in radians.

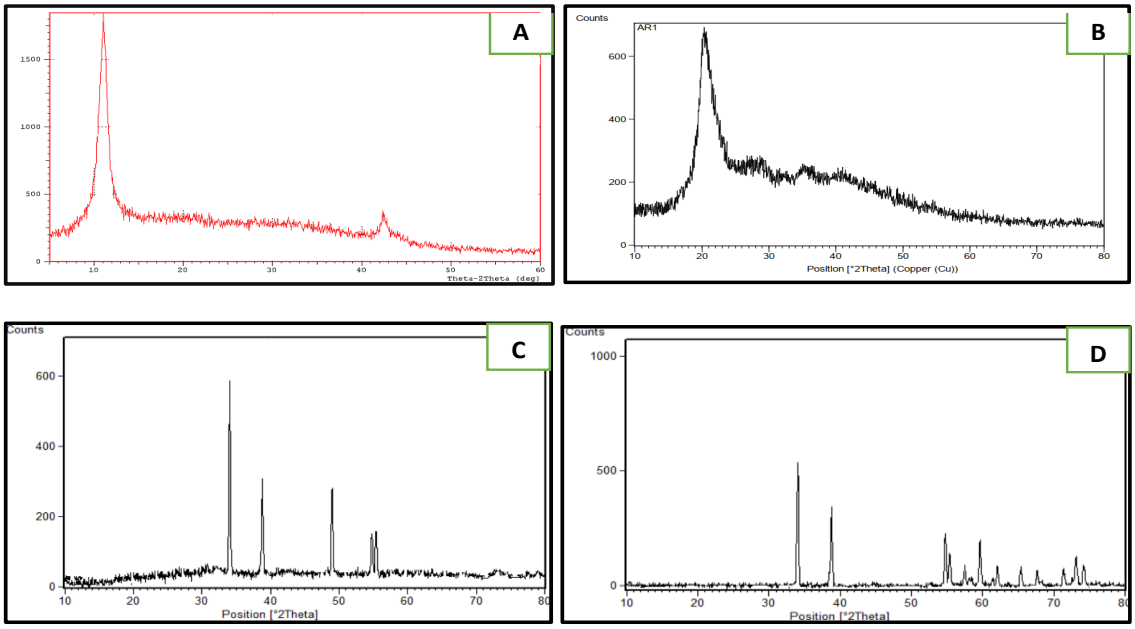

Fig. 3. XRD spectra of (A)NGO, (B) NGO-CS, (C) NGO-M and (D) NGO-C composites

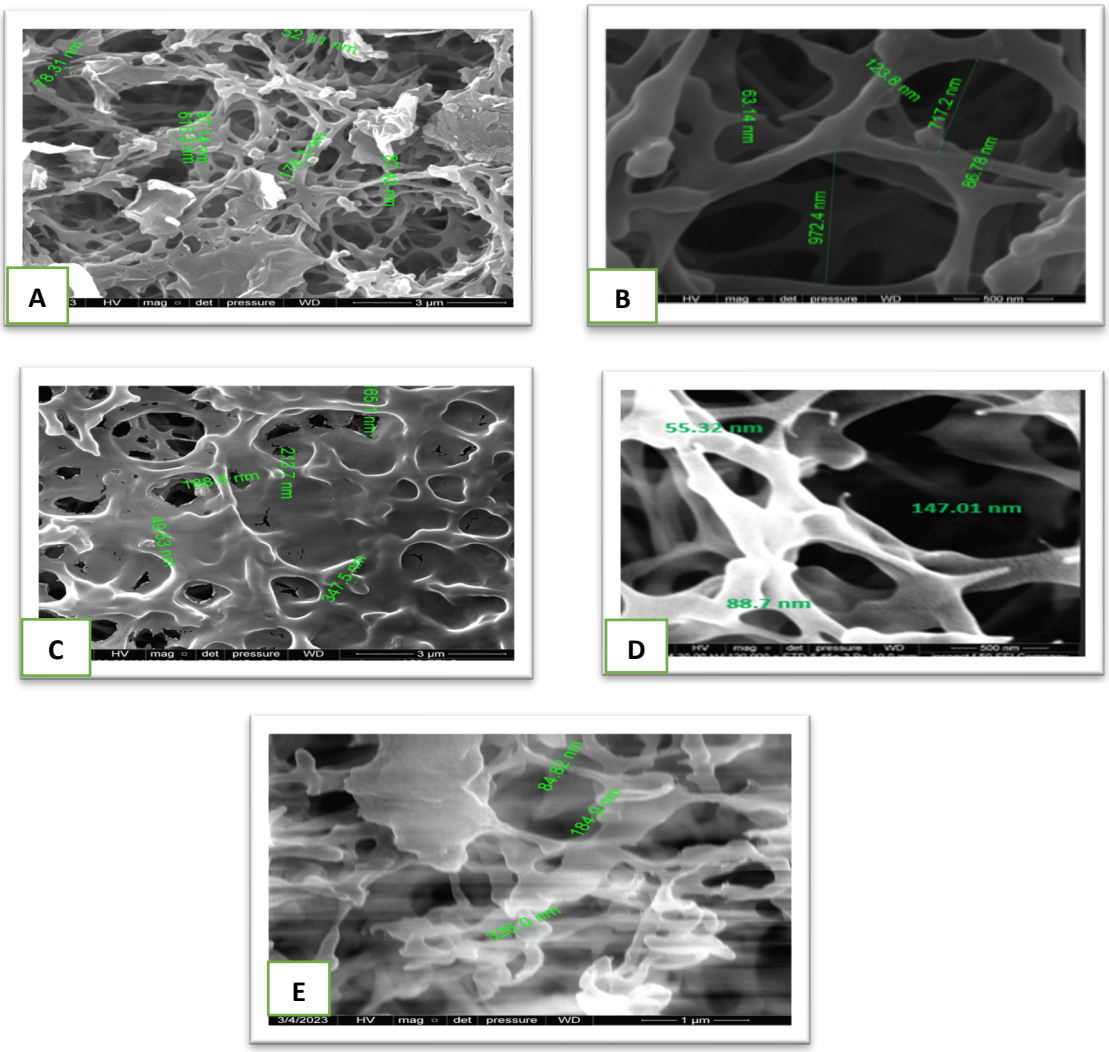

Fig. 4. FESEM image of (A) NGO, (B) CS, (C) NGO- CS, (D) NGO- M, (E) NGO- C composite

The average particle sizes of synthesized NGO, NGO-CS, NGO-M and NGO-C composites are (7.4, 10.8, 16.83 and 19.52 nm) respectively.

Field Emission Scanning Electron Microscopy (FESEM)

The FESEM was used to study the surface morphology of NGO-CS, CS, NGO-M and NGO-C composites membranes, where the corrugation shape is observed of nanosheets. The NGO membrane contains a high porosity [12], and the range of pores size (52.31-613.2) nm at different scales was clear as shown in Fig. 4 (A). The CS membrane contains a high porosity, the range of pores size (63.14-972.4) nm as shown in Fig. 4 (B). FESEM pictures of the GO-CS composite show no visible CS particles, which suggests that the CS chains are distributed uniformly across the NGO sheets[28] [29]. The interconnected pores enable the diffusion of solute throughout the composite the range pores size (49.53-347.5) nm as shown in Fig. 4 (C). The NGO-M and NGO-C membranes contain a high porosity, the range of particle size (84.8-326.0) nm and (55.32-147.01) respectively, as shown in Fig. 4 (D) and (E). Fewer wrinkles on the nanosheet surfaces have more sensitivity and better recovery [30].

Zeta Potential Analysis

Zeta potentials investigate how a particle's surface charge influences the aggregation of nanomaterials and the adsorption of ions onto

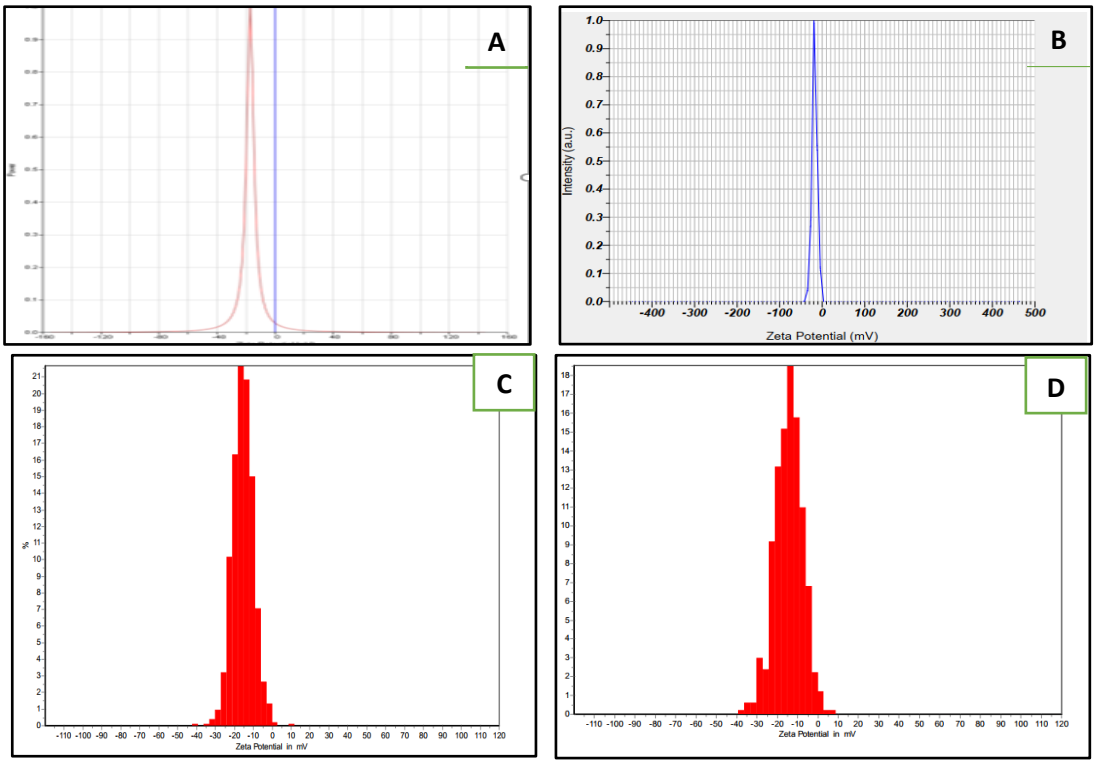

Fig. 5. Zeta potential of (A)NGO, (B) NGO-CS, (C) NGO-M and (D) NGO-C composites

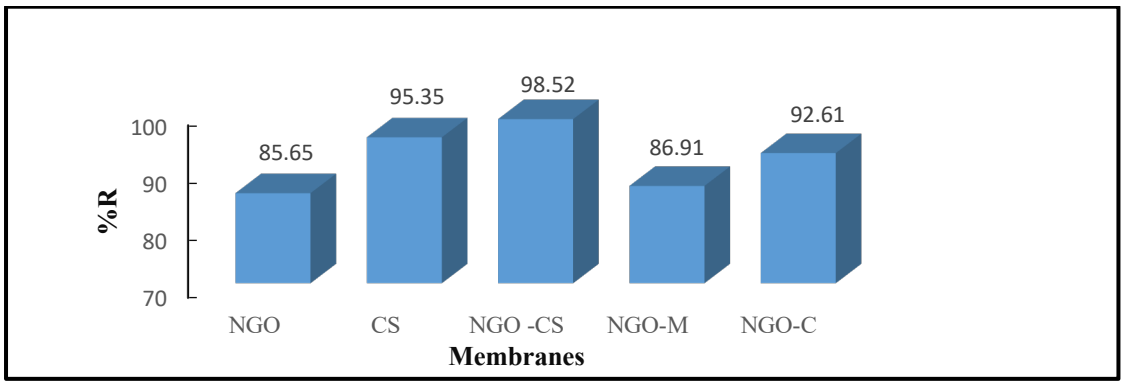

Fig. 6. Removal percentage of BPB dye by NGO, CS, NGO-CS, NGO-M and NGO-C membranes

nanosurfaces [31] [32] [33]. The Zeta potential of NGO, NGO-CS, NGO-M and NGO-C are (-17.17, -17.50, -15.33 and -14.36 mV) respectively as shown in Fig. 5.

Separation of BPB dye by NGO, CS, NGO-CS, NGO-M and NGO-C membranes

The experimental data shows the removal % of BPB dye by the membranes in the order NGO-CS > CS > NGO-C >NGO-M > NGO, the best membrane is NGO-CS, where R (98.5%), as shown in Fig. 6. According to the mechanism study, physical sieving, electrostatic interaction, and hydrogen bonding were the key mechanisms by which this membrane adsorbs dyes [12].

Separation of Ni^{+2}, Cd^{+2}, Co^{+2}, Cu^{+2} and Pb^{+2} ions by NGO, CS, NGO-CS, NGO-M and NGO-C membranes

The standard calibration curves for (Ni^{+2}, Cd^{+2}, Co^{+2}, Cu^{+2} and Pb^{2+}) bivalent ions were determined

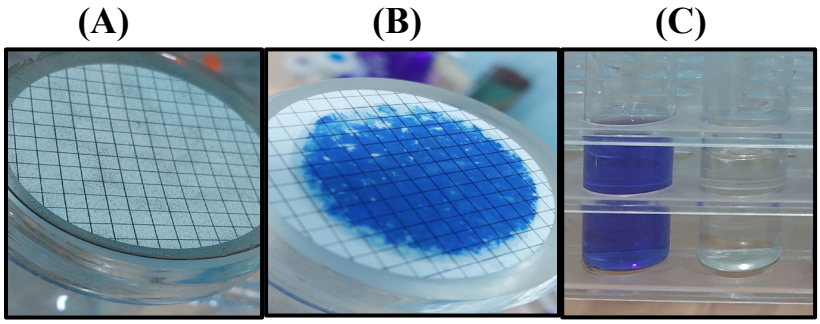

Fig.7. NGO-CS membrane (A, B) before and after separation of BPB dye respectively, (B) Solution of BPB dye before and after separation by NGO-CS membrane

Table 1. The analytical conditions for determination of metal ions by FAA.

Ser.	Ion	(λ_{max}) nm	Detection limit (µg/mL)	Working range (µg/mL)	Silt width (nm)	Flame
1	Co^{+2}	240.7	0.01	2-10	0.2	Air / Acetylene (99%)
2	Ni^{+2}	232.0	0.01	2-10	0.2	Air / Acetylene (99%)
3	Cu^{+2}	324.7	0.004	2-10	0.2	Air / Acetylene (99%)
4	Cd^{+2}	288.8	0.0028	2-10	0.2	Air / Acetylene (99%)
5	Pb^{+2}	217.0	0.012	2-10	0.2	Air / Acetylene (99%)

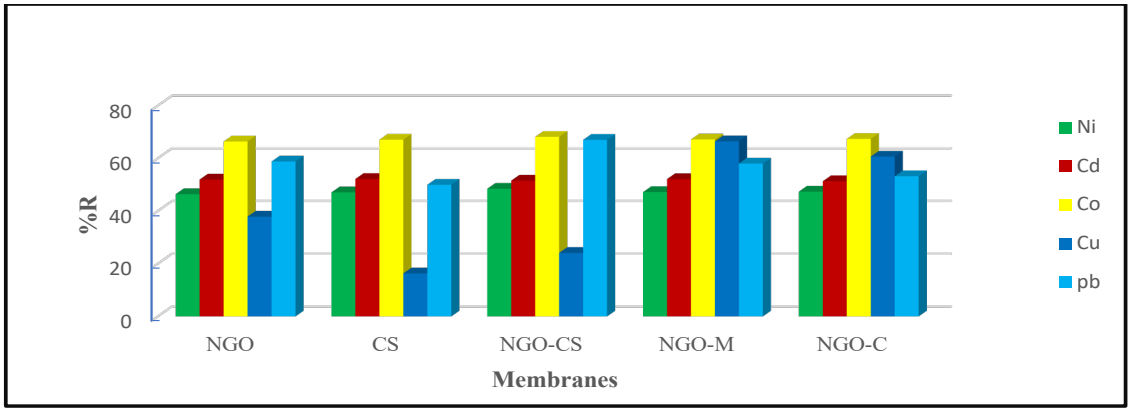

Fig. 8. Removal percentage of Ni^{+2}, Cd^{+2}, Co^{+2}, Cu^{+2} and Pb^{+2} ions by NGO, CS, NGO-CS, NGO-M and NGO-C membranes

by flame atomic absorption spectroscopy (FAAS) according to the manual instructions of (Aurora AI-1200) for each analyte with the limit of detection (LOD) as shown in Table 1.

The result shows that the separation of the heavy metal ions by the membranes exhibits fluctuation and irregularity, the percentage of Ni^{+2} and Co^{+2} ions removal by the membranes were in the order NGO- CS > NGO- C >NGO- M > CS > NGO, the best membrane is NGO- CS, R% (48.47%) and (68.17%) respectively. While, Cd^{+2} ions follow the order CS > NGO- M > NGO > NGO- CS > NGO- C, the best membrane is CS, where R% (52.20 %). The Cu^{+2} ions follow the order NGO- M > NGO- C

Table 2. Recovery percentages of Ni^{+2}, Cd^{+2}, Co^{+2}, Cu^{+2} and Pb^{+2} ions by NGO, CS, NGO-CS, NGO-M and NGO-C membranes

Membranes	Recovery %				
	Ni^{+2}	Cd^{+2}	Co^{+2}	Cu^{+2}	Pb^{+2}
NGO	46.43	51.97	66.43	37.91	58.82
CS	47.10	52.20	67.10	16.35	50.00
NGO-CS	48.47	51.57	68.17	24.13	67.04
NGO-M	47.20	52.14	67.20	66.47	58.03
NGO-C	47.38	51.33	67.38	60.68	53.21

> NGO> NGO- CS> CS, and the best membrane is NGO-M, where with R% (66.47%). On the other hand, Pb^{+2} ions follow the order NGO-CS > NGO >NGO-M > NGO-C > CS, and the best membrane is NGO-CS with R% (67.04%), as shown in Fig. 8.

CONCLUSION

The following composites (NGO-CS, NGO-M, NGO-C) have been created, the amine group in chitosan polymers, amino acids (methionine and cysteine) are binding to the carboxylic acid and the epoxide groups on the surface of nano-graphene oxide, as indicated by FT-IR analysis**.** The pores distribution in the membranes is irregular, and the sizes are heterogeneous, varying from one membrane to another, and even within the same membrane. The removal percentage of BPB dye by these membranes is high resulting from electrostatic interactions between the BPB dye molecules and the negatively charged surface of the membranes, in contrast to the removal percentage of trace heavy metal ions, as the ions have much smaller diameters than the pore diameters of the membrane, in addition to the electrostatic interaction between the dual positive charge ions and negative charge of the surface membranes related toto zeta potential, Additionally, coordination bonds may also form.

ACKNOWLEDGMENT

The authors would like to thank the staff of Department of Chemistry, college of Science at University of Misan for the assistance in providing the chemicals and instrumental analysis.

CONFLICT OF INTEREST

The authors declare that there is no conflict of interests regarding the publication of this manuscript.

REFERENCES

1. Sharma S, Bhattacharya A. Drinking water contamination and treatment techniques. Applied Water Science. 2016;7(3):1043-1067.
2. Sharma SK, Mahiya S, Lofrano G. Removal of divalent nickel from aqueous solutions using Carissa carandas and Syzygium aromaticum: isothermal studies and kinetic modelling. Applied Water Science. 2015;7(4):1855-1868.
3. Benouis K, khane Y, Ahmed T, Albukhaty S, Banoon S. Valorization of diatomaceous earth as a sustainable eco-coagulant for wastewater treatment: optimization by response surface methodology. Egyptian Journal of Chemistry. 2022;0(0):0-0.
4. Pradeep T, Anshup. Noble metal nanoparticles for water purification: A critical review. Thin Solid Films. 2009;517(24):6441-6478.
5. Kant R. Textile dyeing industry an environmental hazard. Natural Science. 2012;04(01):22-26.
6. Lellis B, Fávaro-Polonio CZ, Pamphile JA, Polonio JC. Effects of textile dyes on health and the environment and bioremediation potential of living organisms. Biotechnology Research and Innovation. 2019;3(2):275-290.
7. Hussain S, Khan N, Gul S, Khan S, Khan H. Contamination of Water Resources by Food Dyes and Its Removal Technologies. Water Chemistry: IntechOpen; 2020.
8. de Souza PR, do Carmo Ribeiro TM, Lôbo AP, Tokumoto MS, de Jesus RM, Lôbo IP. Removal of bromophenol blue anionic dye from water using a modified exuviae of Hermetia illucens larvae as biosorbent. Environmental Monitoring and Assessment. 2020;192(3).
9. Robinson T, McMullan G, Marchant R, Nigam P. Remediation of dyes in textile effluent: a critical review on current treatment technologies with a proposed alternative. Bioresour Technol. 2001;77(3):247-255.
10. Karim Z, Mathew AP, Grahn M, Mouzon J, Oksman K. Nanoporous membranes with cellulose nanocrystals as functional entity in chitosan: Removal of dyes from water. Carbohydr Polym. 2014;112:668-676.
11. Werber JR, Osuji CO, Elimelech M. Erratum: Materials for next-generation desalination and water purification membranes. Nature Reviews Materials. 2016.

12. Wang Z, Wu A, Colombi Ciacchi L, Wei G. Recent Advances in Nanoporous Membranes for Water Purification. Nanomaterials. 2018;8(2):65.
13. Han Y, Xu Z, Gao C. Ultrathin Graphene Nanofiltration Membrane for Water Purification. Adv Funct Mater. 2013;23(29):3693-3700.
14. Rabeea Banoon Z, Kareem A. Al-Lami A, Abbas AM, Al-Shakban M, A. A. Balboul B, Gad M, et al. Asymmetrical liquid crystals synthesis for effective sensing: Fluorescence investigations. Results in Chemistry. 2023;6:101166.
15. Chen J, Yao B, Li C, Shi G. An improved Hummers method for eco-friendly synthesis of graphene oxide. Carbon. 2013;64:225-229.
16. Preconcentration of trace amount Cu(II) by solid-phase extraction method using activated carbon based ion-imprinted sorbent. TURKISH JOURNAL OF CHEMISTRY. 2021.
17. Frindy S, Primo A, Ennajih H, el kacem Qaiss A, Bouhfid R, Lahcini M, et al. Chitosan–graphene oxide films and CO 2 -dried porous aerogel microspheres: Interfacial interplay and stability. Carbohydr Polym. 2017;167:297-305.
18. Divya K, Jisha MS. Chitosan nanoparticles preparation and applications. Environ Chem Lett. 2017;16(1):101-112.
19. Croitoru A-M, Ficai A, Ficai D, Trusca R, Dolete G, Andronescu E, et al. Chitosan/Graphene Oxide Nanocomposite Membranes as Adsorbents with Applications in Water Purification. Materials. 2020;13(7):1687.
20. A Low-Cost Biomimetic Heterostructured Multilayer Membrane with Geopolymer Microparticles for Broad-Spectrum Water Purification. American Chemical Society (ACS).
21. Radey HH, Naijm SS. Surface functionalization of nano graphene oxide by amino acid. International journal of health sciences. 2022;6(S1):941-951.
22. Sankara Narayanan TSN, Jegannathan S, Ravichandran K. Corrosion resistance of phosphate coatings obtained by cathodic electrochemical treatment: Role of anode–graphite versus steel. Prog Org Coat. 2006;55(4):355-362.
23. Ho J, Al-Deen FMN, Al-Abboodi A, Selomulya C, Xiang SD, Plebanski M, et al. N,N′-Carbonyldiimidazole-mediated functionalization of superparamagnetic nanoparticles as vaccine carrier. Colloids Surf B Biointerfaces. 2011;83(1):83-90.
24. Al-Abboodi A, Albukhaty S, Sulaiman GM, Al-Saady MAAJ, Jabir MS, Abomughaid MM. Protein Conjugated Superparamagnetic Iron Oxide Nanoparticles for Efficient Vaccine Delivery Systems. Plasmonics. 2023;19(1):379-388.
25. Justin R, Chen B. Characterisation and drug release performance of biodegradable chitosan–graphene oxide nanocomposites. Carbohydr Polym. 2014;103:70-80.
26. Stobinski L, Lesiak B, Malolepszy A, Mazurkiewicz M, Mierzwa B, Zemek J, et al. Graphene oxide and reduced graphene oxide studied by the XRD, TEM and electron spectroscopy methods. J Electron Spectrosc Relat Phenom. 2014;195:145-154.
27. Muda MS, Kamari A, Bakar SA, Yusoff SNM, Fatimah I, Phillip E, et al. Chitosan-graphene oxide nanocomposites as water-solubilising agents for rotenone pesticide. J Mol Liq. 2020;318:114066.
28. Al-Abboodi A, Fu J, Doran PM, Tan TTY, Chan PPY. Injectable 3D Hydrogel Scaffold with Tailorable Porosity Post-Implantation. Advanced Healthcare Materials. 2013;3(5):725-736.
29. Chen Y, Chen L, Bai H, Li L. Graphene oxide–chitosan composite hydrogels as broad-spectrum adsorbents for water purification. J Mater Chem A. 2013;1(6):1992-2001.
30. Xu Y, Nguyen Q, Malekahmadi O, Hadi R, Jokar Z, Mardani A, et al. Synthesis and characterization of additive graphene oxide nanoparticles dispersed in water: Experimental and theoretical viscosity prediction of non-Newtonian nanofluid. Mathematical Methods in the Applied Sciences. 2020.
31. Al-Abboodi A, Mhouse Alsaady HA, Banoon SR, Al-Saady M. Conjugation strategies on functionalized iron oxide nanoparticles as a malaria vaccine delivery system. Bionatura. 2021;3(3):2009-2016.
32. Hussein LM, Hasan AY. The Antibacterial Activity of the Biosynthesized Copper Oxide Nanoparticles by Lantana camara Flowers Extract Against Some Bacterial Isolated from Burns. Al-Mustansiriyah Journal of Science. 2023;33(5):39-52.
33. Aldujaili NH, Banoon SR. ANTIBACTERIAL CHARACTERIZATION OF TITANIUM NANOPARTICLES NANOSYNTHESIZED BY STREPTOCOCCUS THERMOPHILUS. Periódico Tchê Química. 2020;17(34):311-320.